

Lehmann Jascha (Orcid ID: 0000-0003-3261-6750)
Kretschmer Marlene (Orcid ID: 0000-0002-2756-9526)
Schauberger Bernhard (Orcid ID: 0000-0001-7917-0392)

Potential for early forecast of Moroccan wheat yields based on climatic drivers

J. Lehmann¹, M. Kretschmer², B. Schauburger¹, and F. Wechsung¹

¹Potsdam Institute for Climate Impact Research (PIK), Member of the Leibniz Association, Potsdam, Germany

²University of Reading, Reading, United Kingdom

Corresponding author: Jascha Lehmann (jlehmann@pik-potsdam.de)

Key Points:

- Moroccan wheat yield anomalies are hindcasted four months before harvest based on climate precursors.
- Precursors are extracted from gridded fields of climate variables using physically guided causal discovery algorithms.
- The detected causal interactions are physically meaningful and consistent with documented teleconnections in the climate system.
-

Abstract

Wheat production plays an important role in Morocco. Current wheat forecast systems use weather and vegetation data during the crop growing phase, thus limiting the earliest possible release date to early spring. However, Morocco's wheat production is mostly rainfed and thus strongly tied to fluctuations in rainfall, which in turn depend on slowly evolving climate dynamics. This offers a source of predictability at longer timescales. Using physically-guided causal discovery algorithms we extract climate precursors for wheat yield variability from gridded fields of geopotential height and sea surface temperatures which show potential for accurate yield forecasts already in December, with around 50% explained variance in an out-

This article has been accepted for publication and undergone full peer review but has not been through the copyediting, typesetting, pagination and proofreading process which may lead to differences between this version and the Version of Record. Please cite this article as 10.1029/2020GL087516

of-sample cross-validation. The detected interactions are physically meaningful and consistent with documented ocean-atmosphere feedbacks. Reliable yield forecasts at such long lead times could provide farmers and policy-makers with necessary information for early action and strategic adaptation measurements to support food security.

Plain Language Summary

The per capita consumption of cereals in Morocco is one of the highest in the world placing a significant role to wheat production in the framework of national food security. Early wheat forecasts are crucial to increase the resilience of the agricultural sector to climate risks. So far, operational forecast systems provide first yield estimates in March-April and hence around one month before harvest starts in May. These systems use weather and vegetation data during the crop growing phase thus limiting the earliest possible release date to this very time period. Here, we present a different approach based on causal interactions in the climate system to provide accurate forecasts of year-to-year wheat yield changes already in December. We make use of the fact that wheat production is mostly rainfed and thus strongly coupled to prevailing rain conditions which, in turn, are influenced by slowly evolving circulation patterns and sea surface temperatures in the Atlantic and Pacific Ocean. These links between far-away regions, also known as teleconnections, can last for several months and thus provide predictability at seasonal timescales relevant for strategic adaptation decisions, e.g. regarding crop import planning or the choice and intensity of agronomic practices.

1 Introduction

Agriculture is of particular strategic importance in Morocco. Most of the arable land is devoted to cereals with wheat accounting for the majority of total cereal production and thus playing a key factor for national food security. However, most of the arable land is located in arid or semi-arid regions which are characterized by long dry periods and high year-to-year rainfall variations (Born et al., 2008). Since very little of the arable land is irrigated, this leaves Morocco's wheat production heavily dependent on large fluctuations in rainfall intensities (Berdai et al., 2011). Reliable seasonal forecasts could help in reducing the vulnerability of the Moroccan agriculture to weather risks by enabling timely in-season adaptation. Since the Moroccan climate is projected to become drier and hotter with ongoing global warming, such forecasts will likely become even more important in the future (Born et al., 2008; Filahi et al., 2017).

Operational yield forecasting systems provide estimates at lead times of a few days up to three months before harvest in May-June. Provisional forecasts are released every year by the Crop Growth Monitoring System – Morocco (CGMC-MAROC) in April and then constantly revised over the course of the season. CGMC-MAROC uses a physical crop growth model combined with statistical models (Bernardi, 2016; Bregaglio et al., 2014). Based on empirical regression models using weather and vegetation data Balaghi et al. (2008) accurately forecast grain yields as early as of March. Yet, both approaches use the Normalized Difference Vegetation Index (NDVI) during mid-season of the growing phase which limits the earliest possible release date to early spring.

Longer lead times may be achieved through utilization of remote climatic drivers which influence rainfall variability over Morocco and thus wheat production. Total annual wheat yields are significantly correlated to accumulated rainfall during the rainy season lasting from September to May (De Wit et al., 2013). Intra-seasonal rainfall variability in turn is influenced by large-scale climate dynamics including atmospheric circulation patterns and sea surface temperatures over the Pacific and Atlantic Ocean which may persist over months allowing for skillful forecasts of rainfall and NDVI at extended lead times (Jarlan et al., 2014; Knippertz et al., 2003; Rodríguez-Fonseca et al., 2006). The most prominent mode of large-scale variability in the Atlantic, the North Atlantic Oscillation (NAO), has been shown to directly influence the early stage of Moroccan wheat growth in December by shaping the storm tracks which bring moist air from the Atlantic Ocean to the land (Jarlan et al., 2014). Moreover, indirect influences on Moroccan rainfall may occur via atmospheric teleconnections; wave trains, for instance, can emerge from sea surface temperature forcing and may lead to temperature and rainfall changes in far-away regions downstream of the wave (Schlueter et al., 2019; Shaman & Tziperman, 2011).

Tapping into this potential source of forecasting rainfall and thus Moroccan wheat yields, we here apply a physically motivated approach based on causal discovery algorithms (Runge et al., 2019) to find causal climate precursors for interannual wheat yield variability at least four months before harvest. Previous studies have successfully applied the methodology of causal

precursors to forecast extreme stratospheric polar vortex states relevant for mid-latitude winter weather (Kretschmer et al., 2017) and the Indian summer monsoon intensity (Di Capua et al., 2019).

2 Data

Moroccan wheat yield (MWY) data. Nationally aggregated annual wheat yield data for the time period 1979-2017 is taken from the website of the Food and Agriculture Organization (FAO) (FAOSTAT, 2017) with wheat yields given in hectograms per hectare (hg/ha). Annual anomalies are calculated based on the difference to the yield in the previous year (first differences) thereby removing possible linear trends. See the Supporting Information (SI) for the original time series of absolute values (Fig. S1). We chose to forecast yields instead of total production because yields are more directly correlated with the climate whereas the crop area needed to calculate total production also depends on socio-economic influences. If production is required, a wheat area mask can be derived from static crop masks like SPAM (Fritz et al., 2015) or MIRCA2000 (Portmann et al., 2010) or from harvested area of last season.

Climate data. Precursors are derived from two climate variables: sea surface temperature (SST) and geopotential height at 500 hPa (Z500), with the latter being a commonly used level to describe high and low pressure systems in the mid troposphere. We selected these climate variables because they were shown to be linked to Moroccan winter climate and/or wheat yields (e.g. Jarlan et al., 2014; Knippertz et al., 2003; Tuel & Eltahir, 2018). Both climate variables are taken from the ERA5 reanalysis product provided on a $1^\circ \times 1^\circ$ longitude-latitude grid covering the time period 1979-2017 at monthly time resolution (Hersbach et al., 2019). Similarly, as for the MWY time series, monthly climate anomalies are calculated at each grid cell by calculating the difference to the same month of the previous year. Due to the first differences approach for anomaly calculation and the wheat growing season lasting from November to June, the analysis is limited to the years 1981-2017.

3 Building the statistical forecast model – a three step approach

Building the forecast model consists of three steps: (1) defining potential precursors from gridded climate variables by hierarchical clustering of correlation maps, (2) selecting causal precursors from potential precursors using causal discovery algorithms and (3) applying multiple-linear regressions on observed yield anomalies using causal precursor time series.

Step 1: Define potential precursors

Potential precursors are defined as confined regions of a climate variable whose changes precede changes in the target variable, i.e. nationally aggregated MWY anomalies. In a first step, pairwise correlation analyses are conducted between MWY anomalies and lagged time series of monthly Z500 and SST anomalies at each grid cell of the gridded globe between 90°N and 20°S to include possible teleconnections from the northern hemisphere and the tropics. Thereby, statistical significance at the grid cell level is defined at the 2% threshold (two-tailed p-value < 0.02). Using two climate variables (Z500 and SST) and four time lags (September to December) thus leads to eight correlation maps from which potential

precursors are extracted. Potential precursors are defined by grouping significantly correlated grid cells of the same correlation sign using Density-Based Spatial Clustering of Applications with Noise (DBSCAN, Ester et al., 1996; Schubert et al., 2017). In DBSCAN a radius of 300 km is chosen to define neighboring grid cells which is found to produce regions of reasonable sizes and spatial separation.

Step 2: Select causal precursors from potential precursors

So far potential precursor regions have been identified which are correlated with the target variable MWY. These lagged correlations, however, do not necessarily imply causation. Non-causal, spurious correlations can emerge from indirect links, common drivers or autocorrelation effects. To remove such spuriously correlated precursors we apply a multivariate causal discovery algorithm (Runge et al., 2019). The algorithm uses partial correlations to iteratively check whether the link between a given potential precursor and the target variable can be explained by any combination of the remaining potential precursors. If this is the case, i.e. if the given potential precursor is conditionally independent from the target variable, then this potential precursor is removed. Otherwise, it is considered as a causal precursor. A detailed step-by-step description of this causal selection step can be found in Kretschmer et al. (2016). Despite the thorough selection process the definition of causality given here, like any causal interpretation, rests on several underlying assumptions (J. Runge, 2018). In this sense, causal precursors as defined in this study should be understood as climatic indices which exhibit a significant, time-lagged linear dependence with MWY anomalies that cannot be explained by any other identified potential precursor or combination of those.

The combination of step 1 and step 2 of the method part was first introduced by Kretschmer et al. (2017) as the response-guided causal precursor detection. Here, we apply the same method albeit with the modification of clustering significantly correlated grid cells in step 1 in contrast to merging only directly neighboring grid cells. This has shown to improve the robustness of detecting potential precursor regions.

Step 3: Build the forecast model based on causal precursors

In the last step we perform a multiple-linear regression between the anomaly time series of the selected causal precursors and MWY anomalies to build the forecast model in the form $MWY_{\text{forecast}} = \alpha + \sum_i^n \beta_i \cdot CP_i + \varepsilon_i$, where α is the intercept, β_i is the parameter of the i -th causal precursor (CP_i) with error term ε_i and n is the total number of causal precursors.

4 Results

4.1 Extracting causal precursors from climate data

In total 61 potential precursors are extracted (step 1) from the pairwise correlation analysis between the gridded climate variables and MWY anomalies indicating both positive as well as negative correlations (respective red and blue regions with contours in Fig. 1). Potential precursors are found in each correlation map with spatial patterns of Z500 precursors showing larger differences between time lags compared to SST as expected from higher

variability in the atmosphere. Correlation maps are robust with similar regions found for different significance thresholds and subsamples of the studied time period (see details in SI, Fig. S2).

Amongst all 61 potential precursors only five are found to be causally linked to MWY anomalies following step 2 of the model building approach (Fig. 2). These causal precursors include a region of negatively correlated Z500 anomalies over Central to Southwestern Europe in November and December suggesting that Z500 anomalies in these months provide relevant, independent information for MWY. Otherwise, the applied causal discovery algorithm should have eliminated one of the two precursors during the conditional independence test. Consistently, the correlation between both Z500 regions is only weak (Pearson correlation coefficient of $r=0.36$, Fig. S3). A second causal precursor is found in December which refers to positively correlated SST anomalies in the Coral Sea northwest of Australia. Two causal precursors emerge in October and relate to positively correlated SST anomaly fields – one in the North Atlantic off the East Cost of the USA and the other in the tropical Atlantic along the western African coastline. In September no causal precursor for MWY is identified. We test the robustness of the causal selection step by altering significance thresholds and applying them to subsamples of the data and overall find consistent results (see detailed discussion in SI, Fig. S4). Particularly, causal precursors 1-4 only show little sensitivity to the chosen settings.

4.2 Validation of the Moroccan wheat yield hindcasts

Hindcasted yield anomalies strongly correlate with observed anomalies, explaining 88% of the observed yield variance over the full time period with a root mean square error (rmse) of 2530 hg/he (Fig. 3a). Thereby, each causal precursor contributes a similar individual share of 15-25% to the total explained variance (Fig. S5) as computed from variance decomposition of the multiple-linear regression model (Grömping, 2007). Oscillating MWY variability over the last decade seems to be driven by similar variability of the causal Z500 precursor regions in December and November (Fig. S6) which is in line with increased correlation strength over time between both precursors and MWY (Fig. S7). In contrast, correlation strength between MWY and the causal SST precursor in the equatorial Atlantic starts at a high level of around $r=0.8$ and then decreases to around $r=0.4$ in 2010. The transition phase when the correlation of MWY with the Z500 precursors becomes stronger than with the SST precursor corresponds to the time period where hindcasts diverge most from observations (1999-2003) and may thus play a role for this discrepancy. Analyses of the hindcast residuals confirm that the assumptions of a multiple-linear regression model are fulfilled; that is that residuals are characterized by a mean value of zero, constant variance (homoscedasticity), no significant auto-correlation and follow a normal distribution (Fig. S8).

The regression model is robust with respect to its regression parameters of the identified causal precursors. To show this we divide the time series into two parts; regression parameters are derived from the training period (19 years, 1981-1999) and then used to

hindcast MWY anomalies over the test period (18 years, 2000-2017). The explained variance over the training period (91%, $\text{rmse} = 2100 \text{ hg/he}$) is high and similar to the explained variance over the test period (85%, $\text{rmse} = 3170 \text{ hg/he}$), indicating that the regression model does not suffer from overfitting given the hypothetical case that all five causal precursors were known (Fig. 3b).

We next implement an out-of-sample cross validation to further validate the predictive skill of our hindcast model in the case that causal precursors are not known a priori. For this, we iteratively remove two consecutive years from the time series with the remaining years serving as the training period and the left-out years as the test period. We choose to remove two consecutive years instead of just one to account for the strong year-to-year autocorrelation of the causal precursor time series (Fig. S9). The full hindcast model (step1-3) is then calculated using data from the training period only to ensure that data against which the model skill is validated does not enter any part of the model building process.

Hindcasted yield anomalies from this cross validation still explain 49% ($\text{rmse} = 5330 \text{ hg/ha}$) of the observed variance over the full time period with observations mostly staying within the 95% prediction interval (Fig. 3c). The drop in explained variance is due to the fact that not all five causal precursors are detected in each training period which is primarily due to small changes in the identified potential precursor sets. Repeating the cross-validation using prescribed potential precursors from the full time period increases the explained variance to 76% ($\text{rmse} = 3640 \text{ hg/he}$), Fig. S10).

4.3 Forecasting wheat yields and comparison to other statistical methods

We next assess the potential of our approach to forecast interannual MWY changes and find it to produce accurate forecasts when operated in a one-step ahead mode. For this, we use climate and yield data from the 25-year period prior to the to-be-forecasted year to build the full forecast model, i.e. to define potential precursors, select causal precursors and derive the regression parameters. Regression parameters are then applied to causal precursor anomalies from the 26th year to produce the forecast. Afterwards the 25-year period is shifted by one year to re-build the complete model used to forecast the next year and so on. This way, possible long-term changes in teleconnections affecting MWY can in principle be captured. The forecast model accurately forecasts MWY anomalies showing the right direction of change in each year and explaining 72% of its variance ($\text{rmse} = 5250 \text{ h/he}$) between 2006 and 2017. Years before 2006 could not be tested because of a required reasonably long training period prior to the forecasted year. Observed yield anomalies are within the 95% prediction interval except for 2007 and 2016 where the observed decline in yield is significantly lower than forecasted and in 2009 where the observed yield anomaly is significantly higher.

To assess the added value of our forecast model we compare results to two simple forecast models; one which assumes that the forecasted yield is equal to the average of historical yields plus a linear trend and a second one which sets all forecasts to be the anomaly of the

previous year but inversed in sign (see details in SI, Fig. S11-S12). The latter model has no physical meaning but is motivated by the characteristic time series of strongly alternating yield anomalies. The average+trend model and the previous-year model show some skill in forecasting next year's yield during 2006-2017 ($r^2 = 0.71$ and 0.58 , $rmse = 5840$ and 6000 hg/he, respectively). However, predictive skill drastically decreases in the out-of-sample cross validation with two years omitted in the training phase ($r^2 = 0.29$ and 0.24 , $rmse = 6290$ and 7400 hg/he, respectively), indicating that most of the skill in the forecast mode comes from the strong year-to-year autocorrelation of MWY and causal precursor anomalies. Our causal precursor based model outperforms both simple models by a factor of around two with respect to explained variance.

5 Discussion and Conclusions

We have shown that Moroccan wheat yield anomalies which are strongly linked to winter rainfall changes can be robustly predicted using five causal precursors extracted from geopotential height anomalies at 500 hPa and sea surface temperatures. The physical interpretation of the discovered links is discussed in the following.

A clear direct effect can be derived from the November and December geopotential height anomalies over Europe indicated as causal precursors 1 and 3 (see Fig. 2). A high pressure system over this region deflects extratropical storms to the north which bring moist air from the Atlantic Ocean to the land (Hurrell, 1995). In turn, negative geopotential height anomalies would favor more zonal storm tracks leading to more rainfall over Morocco (and thus higher yields) consistent with the negative link we find between the precursors and wheat yields. The center and spatial pattern of the two precursors resemble the southern region of pressure anomalies characteristic for the North Atlantic Oscillation (NAO). Indeed, also the NAO counterpart of positively correlated Z500 anomalies over Greenland/Iceland was identified in the correlation maps (Fig. 1) but not found to add additional information for MWY. A strong link between NAO and Moroccan precipitation has already been reported and used for predictions (El Hamly & Sebbar, 1998; Jarlan, Abaoui, et al., 2014; Knippertz et al., 2003). Here, this region is selected from our data-driven method directly, confirming earlier findings.

The positive correlation between October SST anomalies at the East Coast of the USA (precursor 4, Fig. 2) and changes in wheat yields may arise via extratropical storm track activity. The causal precursor region largely overlaps with a region of strong cyclogenesis of extratropical storms. Cyclogenesis is largely determined by the surface layer and hence by sea surface temperatures (Hoskins & Valdes, 1990). High temperature gradients in this region provide favorable conditions for the creation of extratropical storms and thus increased storm track activity associated with anomalously wet conditions over Europe and North Africa (Lehmann & Coumou, 2015).

A more indirect effect can be assumed from both tropical sea surface temperature precursors on Moroccan winter rainfall and thus wheat yields. There is an extensive body of literature on tropical-extratropical interactions which explain how tropical thermal forcing impacts on

extratropical weather conditions through induced atmospheric responses (see e.g. Robertson & Vitart, 2019 and references therein). The most important tropical-extratropical teleconnection at the subseasonal to seasonal timescale emerges from the Madden-Julian Oscillation (MJO) (Stan et al., 2017; Vitart, 2017). It has been shown that phase 6-7 of the MJO can enhance poleward and vertical Rossby wave propagation leading to negative NAO-like conditions via a stratospheric pathway (Lee et al., 2019) and thus positive precipitation anomalies over western North Africa (Cassou, 2008; Lin et al., 2009). This link is in agreement with December precursor 2 in the West Pacific suggesting that it provides predictability for Moroccan wheat yields via its remote influence on winter rainfall. The reported SST precursor 5 in October is consistent with a documented tropical driver of Moroccan wheat yields. Warming of this region along the western African coastline has been shown to enhance latitudinal moisture transport via changes in trade winds which is important for autumn rainfall in Morocco and thus for the early phase of wheat development (Knippertz et al., 2003).

The reported set of causal precursors is robust over the studied time period. However, for some shorter time intervals only a subsample of the set is found to be significant. Assessing the origin of these differences using data from climate models could give valuable insights into whether this is a statistical artefact or due to actual changes in physical teleconnections. Moreover, albeit all five causal precursors were found to be similarly important to forecast Moroccan wheat yields, each of them may be relevant for different phases of rainfall during the rainy season or rainfall at different locations. For example, it has been suggested that pressure anomalies consistent with precursor 1 are important for early wheat growth (Jarlan, Abaoui, et al., 2014) whereas tropical Pacific SSTs corresponding to precursor 2 are relevant for late-season precipitation (El Hamly & Sebbar, 1998). This should be assessed in subsequent research by linking climate drivers to spatially resolved rainfall over Morocco using the causal discovery algorithm presented in this study. Finally, further insights can be gained by analyzing how teleconnections operating on longer timescales might affect the precursors identified in this study. For example, Lee et al. (2019) showed that the El Niño Southern Oscillation (ENSO) influences the above mentioned MJO-NAO link through modulation of the seasonal mean background state.

Recent research showed the great potential of teleconnections as a source of predictability on subseasonal to seasonal timescales, relevant for a multitude of applications (Dobrynin et al., 2018; Merryfield et al., 2020; White et al., 2017). Here we showed that climatic information can be used to forecast Moroccan wheat yields four months before harvest through its direct link to prevailing rainfall conditions. This would offer release dates 3-5 months earlier compared to current operational forecast systems which use vegetation data and provide first yield estimates in March (Joint Research Centre – Monitoring Agricultural Resources, JRC MARS), April (CGMS-MAROC) or May (United States Department of Agriculture, USDA). Comparison of forecast skill between the different models is nearly impossible due to marked differences in input data, metrics, validation techniques, and even the forecasted output (e.g. yield vs. production). Yet, it is reasonable to assume that forecast accuracy of monthly updated operational forecasts generally improves over the course of the season.

Ideally, our model would thus be used to increase the volume of existing forecast information and extend the lead time for initial estimates. Such long lead times could significantly improve strategic adaptation measures from the state to farm level including early wheat import planning, the application of plant protection materials and fertilizers, and provide humanitarian actors with timely information for early action. The presented method can easily be transferred to other indicators and regions. Yet, we emphasize that expert knowledge, e.g. about appropriate climate precursors, and a careful interpretation of the results is crucial to extract meaningful results.

Acknowledgments and Data

We would like to thank Sem Vijverberg for fruitful discussions and his technical support and Dim Coumou, Christoph Gornott and Giorgia Di Capua for their helpful comments.

We thank the FAO and ECMWF for making their data available. For this study, ERA5 data was retrieved via the Copernicus website (<https://climate.copernicus.eu/climate-reanalysis>) and Moroccan wheat yield via the FAO website (<http://www.fao.org/faostat/en/#data/QC>).

The work was supported by the German Federal Foreign Office through the ClimSec project (OEH: 9482).

References

- Balaghi, R., Tychon, B., Eerens, H., & Jlibene, M. (2008). Empirical regression models using NDVI, rainfall and temperature data for the early prediction of wheat grain yields in Morocco. *International Journal of Applied Earth Observation and Geoinformation*, 10(4), 438–452. <https://doi.org/10.1016/j.jag.2006.12.001>
- Berdai, H., Karrou, M., Chati, M. T., Boutfirass, M., & Bekaou, A. (2011). Irrigation water management in Morocco: a review. In *"Improving Water and Land Productivities in Rainfed Systems, Community-Based Optimization of the Management of Scarce Water Resources in Agriculture in CWANA. Report No. 8.*
- Bernardi, M. (2016). Crop Yield Forecasting in Morocco. *Food and Agriculture Organization of the United Nations*, (February).
- Born, K., Fink, A. H., & Paeth, H. (2008). Dry and wet periods in the northwestern Maghreb for present day and future climate conditions. *Meteorologische Zeitschrift*, 17(5), 533–551. <https://doi.org/10.1127/0941-2948/2008/0313>
- Bregaglio, S., Frasso, N., Pagani, V., Stella, T., Francone, C., Cappelli, G., et al. (2014). New multi-model approach gives good estimations of wheat yield under semi-arid climate in Morocco. *Agronomy for Sustainable Development*, 35(1), 157–167. <https://doi.org/10.1007/s13593-014-0225-6>
- Di Capua, G., Kretschmer, M., Runge, J., Alessandri, A., Donner, R. V., van den Hurk, B., et al.

- (2019). Long-Lead Statistical Forecasts of the Indian Summer Monsoon Rainfall Based on Causal Precursors. *Weather and Forecasting*, 34(5), 1377–1394.
<https://doi.org/10.1175/WAF-D-19-0002.1>
- Cassou, C. (2008). Intraseasonal interaction between the Madden-Julian Oscillation and the North Atlantic Oscillation. *Nature*, 455(7212), 523–527.
<https://doi.org/10.1038/nature07286>
- Dobrynin, M., Domeisen, D. I. V., Müller, W. A., Bell, L., Brune, S., Bunzel, F., et al. (2018). Improved Teleconnection-Based Dynamical Seasonal Predictions of Boreal Winter. *Geophysical Research Letters*, 45(8), 3605–3614.
<https://doi.org/10.1002/2018GL077209>
- Ester, M., Kriegel, H. P., Sander, J., & Xu, X. (1996). A Density-Based Algorithm for Discovering Clusters in Large Spatial Databases with Noise. In: Proceedings of the 2nd International Conference on Knowledge Discovery and Data Mining, Portland, OR, AAAI Press. Elsevier. Elsevier.
- FAOSTAT. (2017). Moroccan Wheat Yield Data. Retrieved from
<http://www.fao.org/faostat/en/#data>
- Filahi, S., Trambly, Y., Mouhir, L., & Diaconescu, E. P. (2017). Projected changes in temperature and precipitation indices in Morocco from high-resolution regional climate models. *International Journal of Climatology*, 37(14), 4846–4863.
<https://doi.org/10.1002/joc.5127>
- Fritz, S., See, L., McCallum, I., You, L., Bun, A., Moltchanova, E., et al. (2015). Mapping global cropland and field size. *Global Change Biology*, 21(5), 1980–1992.
<https://doi.org/10.1111/gcb.12838>
- Grömping, U. (2007). Estimators of relative importance in linear regression based on variance decomposition. *American Statistician*, 61(2), 139–147.
<https://doi.org/10.1198/000313007X188252>
- El Hamly, M., & Sebbar, R. (1998). Towards the seasonal prediction of Moroccan precipitation and its implications for water resources management. *Proceeding of the Abidjan '99 Conference*, 252, 476.
- Hersbach, H., Bell, B., Berrisford, P., Horányi, A., Sabater, J. M., Nicolas, J., et al. (2019). Global reanalysis: goodbye ERA-Interim, hello ERA5. *ECMWF Newsletter*, (159), 17–24.
<https://doi.org/10.21957/vf291hehd7>
- Hoskins, B., & Valdes, P. (1990). On the existence of storm-tracks. *Journal of the Atmospheric Sciences*, 47(15), 1854–1864. [https://doi.org/10.1175/1520-0469\(1990\)047<1854:OTEOST.2.0.CO;2](https://doi.org/10.1175/1520-0469(1990)047<1854:OTEOST.2.0.CO;2)
- Hurrell, J. W. (1995). Decadal trends in the north atlantic oscillation: regional temperatures and precipitation. *Science (New York, N.Y.)*, 269(5224), 676–679.
<https://doi.org/10.1126/science.269.5224.676>

- Jarlan, L., Abaoui, J., Duchemin, B., Ouldbba, A., Tourre, Y. M., Khabba, S., et al. (2014). Linkages between common wheat yields and climate in Morocco (1982-2008). *International Journal of Biometeorology*, 58(7), 1489–1502. <https://doi.org/10.1007/s00484-013-0753-9>
- Jarlan, L., Driouech, F., Tourre, Y., Duchemin, B., Bouyssié, M., Abaoui, J., et al. (2014). Spatio-temporal variability of vegetation cover over Morocco (1982-2008): linkages with large scale climate and predictability. *International Journal of Climatology*, 34(4), 1245–1261. <https://doi.org/10.1002/joc.3762>
- Knippertz, P., Christoph, M., & Speth, P. (2003). Long-term precipitation variability in Morocco and the link to the large-scale circulation in recent and future climates. *Meteorology and Atmospheric Physics*, 83(1–2), 67–88. <https://doi.org/10.1007/s00703-002-0561-y>
- Kretschmer, M., Coumou, D., Donges, J. F., & Runge, J. (2016). Using Causal Effect Networks to Analyze Different Arctic Drivers of Midlatitude Winter Circulation. *Journal of Climate*, 29(11), 4069–4081. <https://doi.org/10.1175/JCLI-D-15-0654.1>
- Kretschmer, M., Runge, J., & Coumou, D. (2017). Early prediction of extreme stratospheric polar vortex states based on causal precursors. *Geophysical Research Letters*, 1–9. <https://doi.org/10.1002/2017GL074696>
- Lee, R. W., Woolnough, S. J., Charlton-Perez, A. J., & Vitart, F. (2019). ENSO Modulation of MJO Teleconnections to the North Atlantic and Europe. *Geophysical Research Letters*, n/a(n/a). <https://doi.org/10.1029/2019GL084683>
- Lehmann, J., & Coumou, D. (2015). The influence of mid-latitude storm tracks on hot, cold, dry and wet extremes. *Scientific Reports*, 5(1), 17491. <https://doi.org/10.1038/srep17491>
- Lin, H., Brunet, G., & Derome, J. (2009). An Observed Connection between the North Atlantic Oscillation and the Madden–Julian Oscillation. *Journal of Climate*, 22(2), 364–380. <https://doi.org/10.1175/2008JCLI2515.1>
- Merryfield, W. J., Baehr, J., Batté, L., Becker, E. J., Butler, A. H., Coelho, C. A. S., et al. (2020). Current and emerging developments in subseasonal to decadal prediction. *Bulletin of the American Meteorological Society*, BAMS-D-19-0037.1. <https://doi.org/10.1175/BAMS-D-19-0037.1>
- Portmann, F. T., Siebert, S., & Döll, P. (2010). MIRCA2000-Global monthly irrigated and rainfed crop areas around the year 2000: A new high-resolution data set for agricultural and hydrological modeling. *Global Biogeochemical Cycles*, 24(1), n/a-n/a. <https://doi.org/10.1029/2008GB003435>
- Robertson, A. W., & Vitart, F. (2019). *Subseasonal to Seasonal Prediction: The Gap Between Weather and Climate Forecasting*. Elsevier.
- Rodríguez-Fonseca, B., Polo, I., Serrano, E., & Castro, M. (2006). Evaluation of the North

- Atlantic SST forcing on the European and Northern African winter climate. *International Journal of Climatology*, 26(2), 179–191. <https://doi.org/10.1002/joc.1234>
- Runge, J. (2018). Causal network reconstruction from time series: From theoretical assumptions to practical estimation. *Chaos: An Interdisciplinary Journal of Nonlinear Science*, 28(7), 075310. <https://doi.org/10.1063/1.5025050>
- Runge, Jakob, Bathiany, S., Bollt, E., Camps-Valls, G., Coumou, D., Deyle, E., et al. (2019). Inferring causation from time series in Earth system sciences. *Nature Communications*, 10(1), 2553. <https://doi.org/10.1038/s41467-019-10105-3>
- Schlueter, A., Fink, A. H., Knippertz, P., & Vogel, P. (2019). A Systematic comparison of tropical waves over northern Africa. Part I: Influence on rainfall. *Journal of Climate*, 32(5), 1501–1523. <https://doi.org/10.1175/JCLI-D-18-0173.1>
- Schubert, E., Sander, J., Ester, M., Kriegel, H. P., & Xu, X. (2017). DBSCAN Revisited, Revisited. *ACM Transactions on Database Systems*, 42(3), 1–21. <https://doi.org/10.1145/3068335>
- Shaman, J., & Tziperman, E. (2011). An Atmospheric Teleconnection Linking ENSO and Southwestern European Precipitation. *Journal of Climate*, 24(1), 124–139. <https://doi.org/10.1175/2010JCLI3590.1>
- Stan, C., Straus, D. M., Frederiksen, J. S., Lin, H., Maloney, E. D., & Schumacher, C. (2017). Review of Tropical-Extratropical Teleconnections on Intraseasonal Time Scales. *Reviews of Geophysics*, 55(4), 902–937. <https://doi.org/10.1002/2016RG000538>
- Tuel, A., & Eltahir, E. A. B. (2018). Seasonal Precipitation Forecast Over Morocco. *Water Resources Research*, 54(11), 9118–9130. <https://doi.org/10.1029/2018WR022984>
- Vitart, F. (2017). Madden—Julian Oscillation prediction and teleconnections in the S2S database. *Quarterly Journal of the Royal Meteorological Society*, 143(706), 2210–2220. <https://doi.org/10.1002/qj.3079>
- White, C. J., Carlsen, H., Robertson, A. W., Klein, R. J. T., Lazo, J. K., Kumar, A., et al. (2017). Potential applications of subseasonal-to-seasonal (S2S) predictions. *Meteorological Applications*, 24(3), 315–325. <https://doi.org/10.1002/met.1654>
- De Wit, A., Hoek, S., Ballaghib, R., El Hairehc, T., & Dong, Q. (2013). Building an operational system for crop monitoring and yield forecasting in Morocco. *2013 2nd International Conference on Agro-Geoinformatics: Information for Sustainable Agriculture, Agro-Geoinformatics 2013*, 466–469. <https://doi.org/10.1109/Argo-Geoinformatics.2013.6621964>

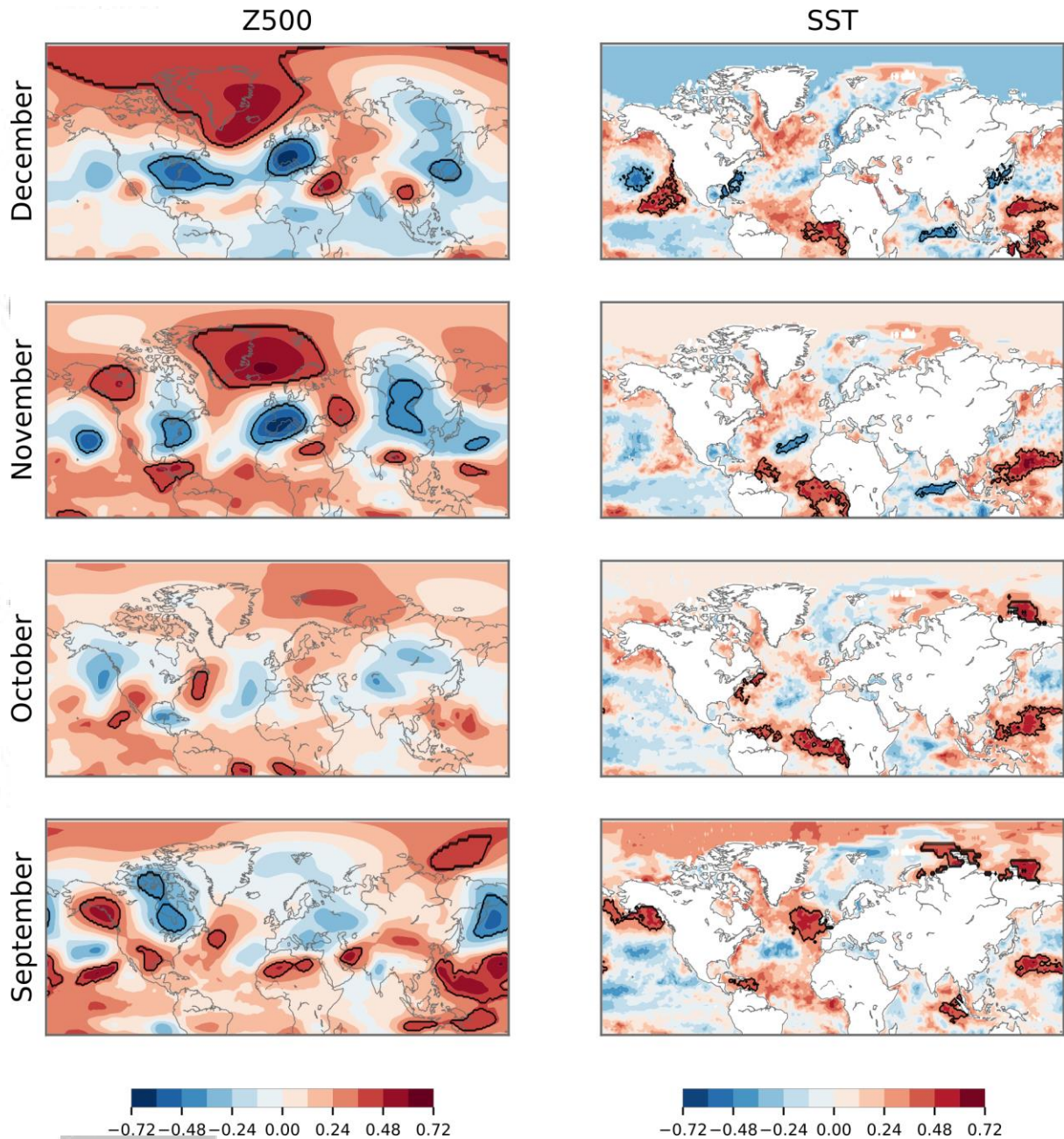


Fig. 1: Potential precursors derived from 500 hPa geopotential height anomaly fields (Z500, left) and sea surface temperature anomaly fields (SST, right). Pairwise correlations are calculated between wheat yield anomalies and the respective climate variable at each grid cell and time lag ranging from lag 4 (December) to lag 7 (September). Significantly correlated grid cells are then aggregated to homogeneous regions using cluster analysis (black contours).

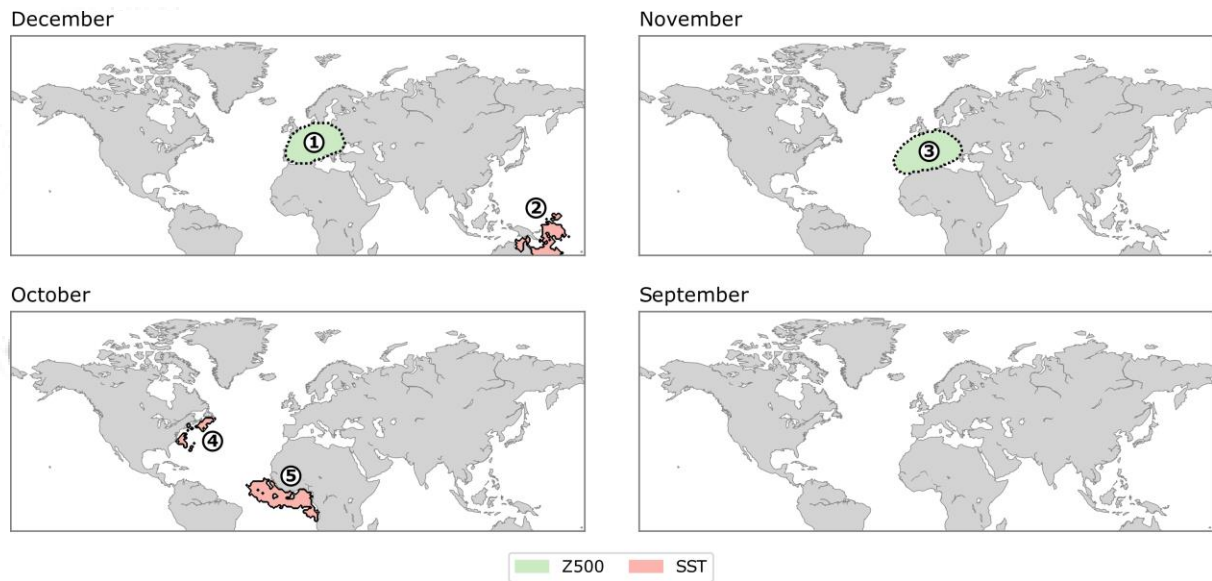


Fig. 2: Causal precursors of Moroccan wheat yield anomalies. Five causal precursor regions are extracted from geopotential height anomaly fields (Z500, green) and sea surface temperature anomalies (SST, red) at different time lags. Contours indicate whether a precursor is positively (solid line) or negatively (dotted line) correlated with yield anomalies.

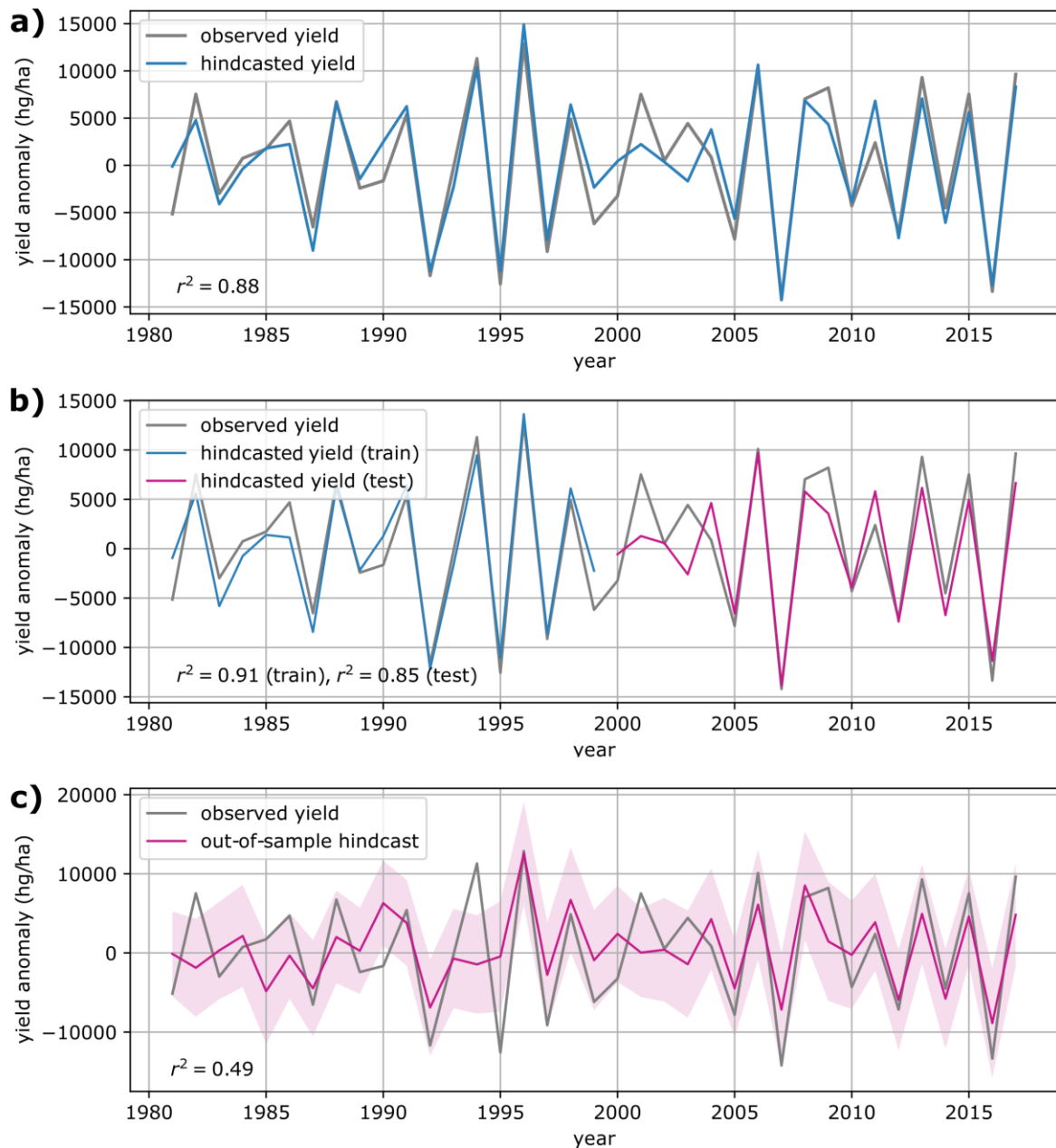


Fig. 3 Hindcasts based on causal precursors. (a) Hindcasted yields strongly correlate with observed yields over the studied time period. (b) Observed and hindcasted yields over a train and a test period with same causal precursors as in (a) and regression parameters calculated from the train period only. (c) Leave-2-out cross validation with strict train-test splitting for all three model building steps. Observed yields mostly stay within the 95% prediction interval.

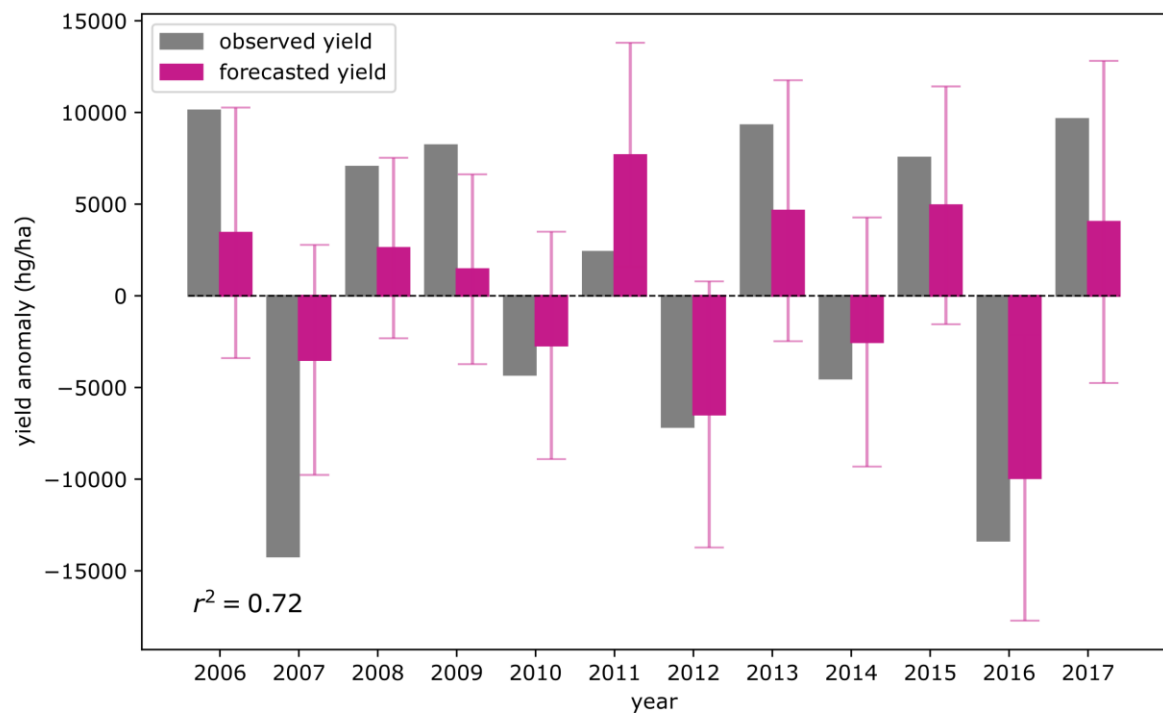


Fig. 4: One-step-ahead forecast. The forecast model is iteratively computed from the 25-year period prior to the to-be-forecasted year. Vertical lines indicate the 95% prediction interval.